World Scientific
www.worldscientific.com

Biomedical applications of Jones-matrix tomography to polycrystalline films of biological fluids

V. A. Ushenko*, A. Yu. Sdobnov†, W. D. Mishalov‡, A. V. Dubolazov*,**,‡‡,
O. V. Olar*, V. T. Bachinskyi§, A. G. Ushenko*, Yu. A. Ushenko*,
O. Ya. Wanchuliak§ and I. Meglinski†,¶,‖,**,††,§§

*Chernivtsi National University
2 Kotsiubynskyi St., Chernivtsi, 58012 Ukraine

†Faculty of Information Technology and Electrical Engineering
University of Oulu, Oulu 90570, Finland

‡Shupyk National Medical Academy of Postgraduate Education
9, Dorogozhytska St., Kyiv, 04112 Ukraine

§Bukovinian State Medical University
3 Theatral Sq., Chernivtsi, 58000 Ukraine

¶Interdisciplinary Laboratory of Biophotonics
National Research Tomsk State University
Tomsk, 634050 Russia

‖Institute of Engineering Physics for Biomedicine (PhysBio)
National Research Nuclear University "MEPhI"
Moscow, 15409 Russia

**Aston Institute of Materials Research
School of Engineering and Applied Science
Aston University, Birmingham, B4 7ET, UK

††School of Life and Health Sciences, Aston University
Birmingham, B4 7ET, UK
‡‡a.dubolazov@chnu.edu.ua
§§igor.meglinski@oulu.fi

Algorithms for reconstruction of linear and circular birefringence-dichroism of optically thin anisotropic biological layers are presented. The technique of Jones-matrix tomography of polycrystalline films of biological fluids of various human organs has been developed and experimentally

§§Corresponding author.

tested. The coordinate distributions of phase and amplitude anisotropy of bile films and synovial fluid taken from the knee joint are determined and statistically analyzed. Criteria (statistical moments of 3rd and 4th orders) of differential diagnostics of early stages of cholelithiasis and septic arthritis of the knee joint with excellent balanced accuracy were determined. Data on the diagnostic efficiency of the Jones-matrix tomography method for polycrystalline plasma (liver disease), urine (albuminuria) and cytological smears (cervical cancer) are presented.

Keywords: Polarization; Fourier optics and signal processing; imaging systems; medical and biological imaging.

1. Introduction

Traditionally, the diagnostics of phase-inhomogeneous object structures are based on the use of various optical techniques, such as spectroscopy, polarimetry, interferometry, etc.[1–5] Mueller-matrix polarimetry (MMP) of optical anisotropy of polydisperse biological objects is one of the most perspective and effective methods for diagnostics in biomedicine.[6] Recent developments and achievements in MMP for the diagnosis of pathological changes in tissues of various human organs have been presented in a number of reviews[7–13] and original[14–17] papers.

For most of the biological objects, the high level of optical radiation depolarization is typical.[18] As a result, determination of the polarization manifestations of various mechanisms of optical anisotropy is a complex and challenging task. To deal with this, the method of Mueller-matrix polar decomposition[19–22] is usually applied. It is important to note that implementation of the decomposition approaches for investigation of complex systems, such as biological tissues, requires comprehensive validation. Particularly, it is necessary to know the influence of the chosen decomposition-derived polarization parameters on the decomposition process, the basis matrices orders, propagation path of multiply scattered photons, detection geometry, etc.[7–10] Therefore, the diagnostic capabilities of MMP technique are highly limited. Moreover, the biopsy operation is necessary for the sample preparations. Since biopsy is a painful and traumatic procedure, the development of minimally invasive methods for biological tissues investigation became a promising and relevant field of research in the last few decades.

The Jones-matrix polarimetry of the polycrystalline structure of optically thin films (attenuation coefficient $\tau < 0.1$) made from biological fluids is one of the effective methods for tissue investigation. Previously, we found that method of direct polarization mapping of microscopic images of biological fluid films (blood plasma, synovial fluid, liquor) is sensitive to pathological changes in human organs.[23–28]

Further development of these studies allowed the Jones-matrix reconstruction of the distributions of linear and circular birefringence of polycrystalline bile films.[29] Thus, this method can be used for diagnostics of Type II diabetes with excellent accuracy. However, the extraction of complete information about all types of anisotropy of polycrystalline films of biological fluids has not yet been realized. The theoretical background for this problem and its possible solution have been presented in a number of papers.[30,31] Therefore, the implementation of this theory for Jones-matrix mapping of biological fluid films is an importent goal for modern biophysics. This technique will allow to obtain new data on the distributions of the phase and amplitude anisotropy parameters. These data will open the prospect of determining the relationship between the transformation of the polycrystalline structure of biological fluid films and the appearance of pathology of various human organs.

Our paper is aimed at the development of the method of Jones-matrix tomography of polycrystalline layers of various types of biological fluids using the samples of bile and synovial fluid from the knee joint.

The choice of these samples is due to the next physical and medical considerations

Physical — Polycrystalline structure of films of such liquids is formed by different types of biochemical crystals. Therefore, a comparative analysis of the obtained Jones-matrix tomography data will make it possible to determine the reliable criteria which are most sensitive to changes in the distributions of the phase and amplitude anisotropy parameters.

The medical — The use of such criteria will expand the functional capabilities of early diagnosis of various pathologies of human organs

- cholelithiasis ("CLS") — Worldwide spread reaches 10%.[32]
- joint infection — An irreversible loss of joint function occurs in 25–50% of patients who have suffered septic arthritis (SA). Mortality varies between 5% and 15%.[33]

These pathologies are impossible to detect at the early stage of disease in most cases. Particularly, precise methods of diagnosis (90–95%) have been developed only for the late stages of CLS formation.[34] Thus, pathology diagnostics with the specified accuracy at the "pre-consecutive" stage remain an open task.

Appropriate diagnostics of joint infection are complex and ambiguous tasks. The clinical picture of the presence of pathology can varies, and its diagnostics methods are nonspecific.[35–37]

Therefore, the development of new, more accurate and fast methods using the novel optical-physical approaches for formation and processing of microscopic images of polycrystalline films of biological fluids of different human organs is an important task in bioimaging.

2. Methods and Materials

2.1. *Basic equations and theoretical remarks*

We start with a brief theoretical description of the Jones-matrix reconstruction (tomography) algorithms for the determination of the parameters of optical anisotropy of polycrystalline films of biological fluids.

The theoretical background of the Jones-matrix tomography has been presented.[30,31] We determine the relationship between the Jones-matrix $\{D\}$, the generalized anisotropy $\mathbf{T}(L_{0;90}; L_{45;135}; C_{\otimes;\oplus})$, the planar layer and its complex elements $d_{ik} = j_{ik} \exp(i(\theta_{ik} - \theta_{11}))$ recorded in the polar form as follows:

$$
\{D\} = \left\| \begin{array}{cc} \cos 0.5T - i\dfrac{L}{T}\sin 0.5T & \dfrac{(C - iL')}{T}\sin 0.5T \\ -\dfrac{(C + iL')}{T}\sin 0.5T & \cos 0.5T + i\dfrac{L}{T}\sin 0.5T \end{array} \right\|,
$$
$$
= K \left\| \begin{array}{cc} j_{11} & j_{12}\exp(i(\theta_{12} - \theta_{11})) \\ j_{21}\exp(i(\theta_{21} - \theta_{11})) & j_{22}\exp(i(\theta_{22} - \theta_{11})) \end{array} \right\|.
$$
$$(1)$$

Here, K is the universal complex constant; T is the modulus of the generalized anisotropy vector

$\mathbf{T}$, $L = \mathrm{LB}_{0;90} - i\mathrm{LD}_{0;90}$, $L = \mathrm{LB}_{45;135} - i\mathrm{LD}_{45;135}$, $C = \mathrm{CB}_{\otimes;\oplus} - i\mathrm{CD}_{\otimes;\oplus}$. They can be rewritten as

$$
K = \left(\begin{array}{c} j_{11}j_{22}\exp(i(\theta_{22} - \theta_{11})) - j_{12}j_{21}\exp(i(\theta_{12} - \theta_{11})) \\ *\exp(i(\theta_{21} - \theta_{11})) \end{array} \right)^{0.5},
$$
$$(2)$$

$$
T = (L_{0;90}^2 + L_{45;135}^2 + C_{\otimes;\oplus}^2)^{0.5},
$$
$$
= \left(\begin{array}{c} (\mathrm{LD}_{0;90} + i\mathrm{LB}_{0;90})^2 + (\mathrm{LD}_{45;135} + i\mathrm{LB}_{45;135})^2 \\ + (\mathrm{CD}_{\otimes;\oplus} + i\mathrm{CB}_{\otimes;\oplus})^2 \end{array} \right)^{0.5},
$$
$$(3)$$

where $\mathrm{LD}_{0,90}$, $\mathrm{LD}_{45,135}$ and $\mathrm{LB}_{0,90}$, $\mathrm{LB}_{45,135}$ are the linear dichroism — birefringence; $\mathrm{CD}_{\otimes;\oplus}$ and $\mathrm{CB}_{\otimes;\oplus}$ are the circular dichroism — birefringence of optically anisotropic component of biological layer for linearly $(0^0 \div 90^0 i 45^0 \div 135^0)$ and circularly right — $(\otimes)$ and left — $(\oplus)$ polarized orthes.

Using Eqs. (1)–(3), the theoretical interrelations $F_{j=1-6}$ between the parameters of linear and circular birefringence-dichroism and elements of the Jones-matrix $\{D\}$ of an optically anisotropic layer can be written as follows:

$$
\begin{cases}
\mathrm{LB}_{0;90} = F_1(j_{ik}, (\theta_{ik} - \theta_{11})), \\
\mathrm{LB}_{45;135} = F_2(j_{ik}, (\theta_{ik} - \theta_{11})), \\
\mathrm{CB}_{\otimes;\oplus} = F_3(j_{ik}, (\theta_{ik} - \theta_{11})), \\
\mathrm{LD}_{0;90} = F_4(j_{ik}, (\theta_{ik} - \theta_{11})), \\
\mathrm{LD}_{45;135} = F_5(j_{ik}, (\theta_{ik} - \theta_{11})), \\
\mathrm{CD}_{\otimes;\oplus} = F_6(j_{ik}, (\theta_{ik} - \theta_{11})),
\end{cases}
$$
$$(4)$$

where j_{ik} is the real part and θ_{ik} are the phase angles of the elements of the Jones-matrix in the polar coordinate system.

In our previous works,[38,39] the technique for Jones-matrix mapping of distributions $j_{ik}(x, y)$ and $\theta_{ik}(x, y)$ was based on probing samples with differently polarized beams $(0^0; 90^0; 45^0; \otimes)$ and the technique for measurement of series of polarization intensity units $(I^{0;90;45;\otimes}_{0;90;45;135;\otimes;\oplus})$ at the points (x, y) of microscopic images of biological fluid films has been developed

$$
\begin{array}{ll}
j_{11} = (I_0^0)^{0.5}; & j_{12} = (I_{90}^0)^{0.5}; \\
j_{21} = (I_{90}^{90})^{0.5}; & j_{22} = (I_0^{90})^{0.5},
\end{array}
$$
$$(5)$$

$$
\Delta\theta_{12;11} = (\theta_{12} - \theta_{11})
$$
$$
= \mathrm{Im}\left[\ln\left(\frac{f_{13} + f_{23} + i(f_{14} + f_{24})}{((f_{11} + f_{21})^2 - (f_{12} + f_{22})^2)^{0,5}} \right) \right];
$$
$$(6)$$

$$\Delta\theta_{21;11} = (\theta_{21} - \theta_{11})$$
$$= \mathrm{Im}\left[\ln\left(\frac{f_{31} + f_{32} + i(f_{41} + f_{42})}{((f_{11} + f_{21})^2 - (f_{21} + f_{22})^2)^{0,5}}\right)\right];$$
$$(7)$$

$$\Delta\theta_{22;11} = (\theta_{22} - \theta_{11})$$
$$= \mathrm{Im}\left[\ln\left(\frac{f_{33} + f_{44} + i(f_{43} - f_{34})}{((f_{11} + f_{22})^2 - (f_{21} + f_{12})^2)^{0,5}}\right)\right].$$
$$(8)$$

Here, f_{ik} are the elements of Mueller matrix of a biological layer

$$
\begin{array}{ll}
f_{11} = 0.5(S_1^0 + S_1^{90}); & f_{31} = 0.5(S_3^0 + S_3^{90}); \\
f_{12} = 0.5(S_1^0 - S_1^{90}); & f_{32} = 0.5(S_3^0 - S_3^{90}); \\
f_{13} = S_1^{45} - f_{11}; & f_{33} = S_3^{45} - f_{31}; \\
f_{14} = S_1^{\otimes} - f_{11}; & f_{34} = S_3^{\otimes} - f_{31}; \\
f_{21} = 0.5(S_2^0 + S_2^{90}); & f_{41} = 0.5(S_4^0 + S_4^{90}); \\
f_{22} = 0.5(S_2^0 - S_2^{90}); & f_{42} = 0.5(S_4^0 - S_4^{90}); \\
f_{23} = S_2^{45} - f_{21}; & f_{43} = S_4^{45} - f_{41}; \\
f_{24} = S_2^{\otimes} - f_{21}; & f_{44} = S_4^{\otimes} - f_{41},
\end{array}
\tag{9}
$$

where $S_{i=1;2;3;4}^{0;90;45;\otimes}$ is the Stokes vector parameters

$$S_{i=1}^{0;45;90;\otimes} = I_0^{0;45;90;\otimes} + I_{90}^{0;45;90;\otimes};$$
$$S_{i=2}^{0;45;90;\otimes} = I_0^{0;45;90;\otimes} - I_{90}^{0;45;90;\otimes};$$
$$S_{i=3}^{0;45;90;\otimes} = I_{45}^{0;45;90;\otimes} - I_{135}^{0;45;90;\otimes};$$
$$S_{i=4}^{0;45;90;\otimes} = I_{\otimes}^{0;45;90;\otimes} - I_{\oplus}^{0;45;90;\otimes}.$$
$$(10)$$

Each biological layer has a complex feature of optical anisotropy.[1] Among them, structural anisotropy (linear birefringence LB and dichroism LD of polycrystalline networks of biological molecules), as well as optical activity (circular birefringence CB and dichroism CD of chiral molecules) are distinguished.[9]

In general, the polarization manifestations of the anisotropy mechanisms mentioned above are described by a set of matrix elements f_{ik}.[43] In fact, at the moment, there is no data on an analytical form of the algorithms of interconnections between the parameters (LB,CB,LD,CD) and the set of elements f_{ik}.

Based on the synthesis of theoretical[30,31] and experimental[23–29,38,39] results, we obtained algorithms for complex Jones-matrix reconstruction of the distributions of both phase (LB$_{0;90}$; LB$_{45;135}$; CB$_{\otimes;\oplus}$) and amplitude (LD$_{0;90}$; LD$_{45;135}$; CD$_{\otimes;\oplus}$)

anisotropy of polycrystalline films of biological fluids

$$
\begin{cases}
\mathrm{LB}_{0;90} = \dfrac{(j_{11} - j_{22}C_1)\sin\left(\frac{D_1}{(D_1+D_2)^{0.5}}\right) - j_{22}C_2\cos\left(\frac{D_2}{(D_1+D_2)^{0.5}}\right)}{(D_1 + D_2)^{0.25}}, \\[4ex]
\mathrm{LB}_{45;135} = \dfrac{(j_{12}A_1 + j_{21}B_1)\sin\left(\frac{D_1}{(D_1+D_2)^{0.5}}\right) - j_{21}B_2\cos\left(\frac{D_2}{(D_1+D_2)^{0.5}}\right)}{(D_1 + D_2)^{0.25}}, \\[4ex]
\mathrm{CB}_{\otimes;\oplus} = \dfrac{(j_{12}A_2 - j_{21}B_2)\sin\left(\frac{D_1}{(D_1+D_2)^{0.5}}\right) - (j_{12}A_2 - j_{21}B_1)\cos\left(\frac{D_2}{(D_1+D_2)^{0.5}}\right)}{(D_1 + D_2)^{0.25}},
\end{cases}
\tag{11}
$$

$$
\begin{cases}
\mathrm{LD}_{0;90} = \dfrac{j_{22}C_2\sin\left(\frac{D_1}{(D_1+D_2)^{0.5}}\right) + (j_{22}C_1 - j_{11})\cos\left(\frac{D_2}{(D_1+D_2)^{0.5}}\right)}{(D_1 + D_2)^{0.25}}, \\[4ex]
\mathrm{LD}_{45;135} = \dfrac{(j_{21}B_2 - j_{12}A_2)\sin\left(\frac{D_1}{(D_1+D_2)^{0.5}}\right) - (j_{12}A_1 + j_{21}B_1)\cos\left(\frac{D_2}{(D_1+D_2)^{0.5}}\right)}{(D_1 + D_2)^{0.25}}, \\[4ex]
\mathrm{CD}_{\otimes;\oplus} = \dfrac{(j_{12}A_1 - j_{21}B_1)\sin\left(\frac{D_1}{(D_1+D_2)^{0.5}}\right) + (j_{12}A_2 + j_{21}B_2)\cos\left(\frac{D_2}{(D_1+D_2)^{0.5}}\right)}{(D_1 + D_2)^{0.25}}.
\end{cases}
\tag{12}
$$

Here

$$
\begin{cases}
A_1 = \dfrac{f_{13} + f_{23}}{((f_{11} + f_{21})^2 - (f_{12} + f_{22})^2)^{0.5}}, \\[3ex]
A_2 = \dfrac{f_{14} + f_{24}}{((f_{11} + f_{21})^2 - (f_{12} + f_{22})^2)^{0.5}},
\end{cases}
\tag{13}
$$

$$
\begin{cases}
B_1 = \dfrac{f_{31} + f_{32}}{((f_{11} + f_{12})^2 - (f_{21} + f_{22})^2)^{0.5}}, \\[3ex]
B_2 = \dfrac{f_{41} + f_{42}}{((f_{11} + f_{12})^2 - (f_{21} + f_{22})^2)^{0.5}},
\end{cases}
\tag{14}
$$

$$
\begin{cases}
C_1 = \dfrac{f_{33} + f_{44}}{((f_{11} + f_{22})^2 - (f_{21} + f_{12})^2)^{0.5}}, \\[3ex]
C_2 = \dfrac{f_{43} + f_{34}}{((f_{11} + f_{22})^2 - (f_{21} + f_{12})^2)^{0.5}},
\end{cases}
\tag{15}
$$

$$
\begin{cases}
D_1 = j_{11}j_{22}C_1 - j_{12}j_{21}(A_1B_1 - A_2B_2), \\
D_2 = j_{11}j_{22}C_2 + j_{12}j_{21}(A_1B_2 + A_2B_1).
\end{cases}
\tag{16}
$$

The found algorithms (Eqs. (9)–(16)) of the Jones-matrix tomography open up the prospects for the experimental investigation and obtaining of new data on the polycrystalline structure of films of biological fluids of human organs with various pathologies and physiological states.

Further, the next equations will be used for generalized linear birefringence (LB) and dichroism (LD)[31] as follows:

$$\text{LB} = (\text{LB}_{0;90}^2 + \text{LB}_{45;135}^2)^{0.5}, \qquad (17)$$

$$\text{LD} = (\text{LD}_{0;90}^2 + \text{LD}_{45;135}^2)^{0.5}. \qquad (18)$$

2.2. Experimental setup

Experimental studies were performed using a classic 2D polarimetry setup. The optical scheme of the polarimeter and the characteristics of its functional parts are described in detail elsewhere.[38,39] In this study, a laser with wavelength $\lambda = 0.6328\,\mu m$ is utilized. In this range of spectra, the absorption of protein complexes is minimal. Thus, the spectral probe makes it possible to study polarization-predominantly phase anisotropy (linear and circular birefringences) of the molecular structures of biological objects. For the purpose of complex radiation of the parameters of phase and amplitude (linear and circular dichroism) anisotropy of the films of biological fluids, we used a "blue" laser diode with a wavelength $\lambda = 0.405\,\mu m$. This probing spectral range allows for simultaneous realization of birefringence-dichroism mechanisms.[40–44]

3. Results and Discussion

3.1. Samples, preparation and statistical validation

The film samples of bile and synovial fluid have been investigated as follows:

- Bile — practically healthy donors ("Norm" — "control" — group (1) and patients with cholelithiasis ("CLS" - "diagnosed" - group (2)
- Synovial fluid — reactive synovitis ("RA"-"control" — group (3) and septic arthritis ("SA" - "diagnosed" — group (4) from the knee joint.

The film samples were made by applying a drop of liquid to an optically homogeneous glass substrate, followed by drying at room ($t \sim 22^0$) temperature.
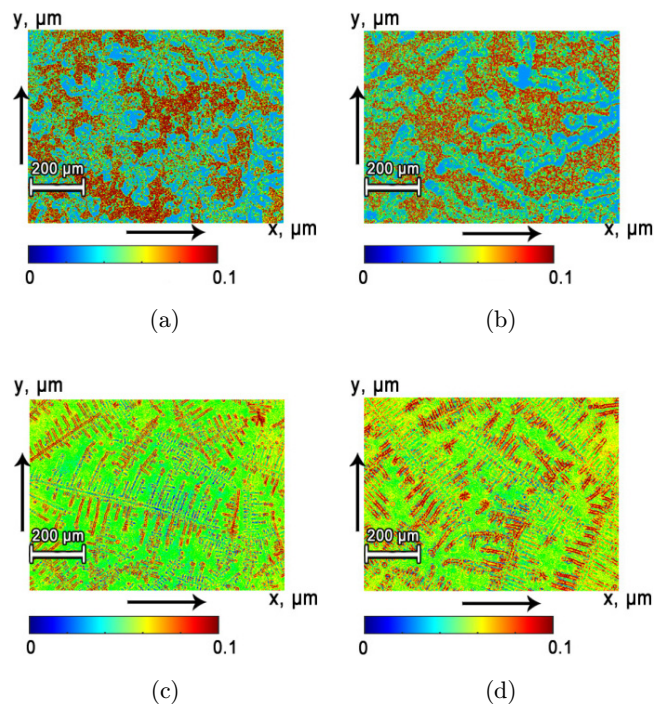

Fig. 1. Microscopic ($4\times$) polarization-visualized images of the optically anisotropic component of bile films (a,b) and synovial fluid (c,d) of control (a,c) and research (b,d) groups.

For all polycrystalline film samples, the single scattering regime ($\tau < 0.01$) has been realized.

Figure 1 shows the polarization visualized in crossed polarizer analyzer, polycrystalline structures of bile films (Groups 1 and 2) and synovial fluid (Groups 3 and 4).

The objects selected for the study combine the similarity of a polycrystalline structure — the presence in all cases of optically anisotropic networks. The biochemical structure of such networks is different. In bile samples, the structure is formed by needle-shaped (LB;LD) crystals of fatty acids, as well as optically active (CB;CD) crystals of cholesterol monohydrate and calcium bilirubinate.[40]

The phase and amplitude anisotropy of the synovial fluid forms various protein complexes (arginine, proline, etc.) with mechanisms of circular anisotropy, as well as fibrin filaments and collagen fibers with linear birefringence-dichroism.[41]

A comparative qualitative analysis of microscopic images revealed the next features (see Fig. 1)

- Polarization-visualized polycrystalline networks of various biological fluids have their own structure;

- The polycrystalline structures of bile and synovial fluid within the control and investigated groups has no significant differences.

Forty-three patients in all groups were determined as reliable using the Statmate software with significant difference $p < 0.05$.

3.2. *Analysis of distributions of phase and amplitude anisotropy*

Obtained (relations (11)–(18)) distributions $\mathrm{OA} \equiv \left\{ {}^{Ph(m \times n);}_{Am(m \times n)} \right.$ were analyzed using the statistical approach.[38,39] Using MATLAB software, we calculated the histograms H(Ph), H(Am) (operator "hist") and statistical moments of the 1st–4th order (operator mean, STD, skewness, excess), which characterize the distributions OA($m \times n$)

$$Z_1 = \frac{1}{K}\sum_{j=1}^{K}\mathrm{OA}_j; \quad Z_2 = \sqrt{\frac{1}{K}\sum_{j=1}^{K}(\mathrm{OA} - Z_1)_j^2},$$

$$Z_3 = \frac{1}{Z_2^3}\frac{1}{K}\sum_{j=1}^{K}(\mathrm{OA} - Z_1)_j^3;$$

$$Z_4 = \frac{1}{Z_2^4}\frac{1}{K}\sum_{j=1}^{K}(\mathrm{OA} - Z_1)_j^4.$$

$$(19)$$

Here, K is the number of pixels in the CCD-camera. These parameters characterize the mean value (Z_1), dispersion (Z_2), skewness (Z_3) and kurtosis or "peak sharpness" (Z_4) of histograms H(Ph) and H(Am).

3.3. *Jones-matrix reconstruction of the polycrystalline structure of biological fluid films*

Figures 2 and 3 show results of the Jones-matrix reconstruction of phase distributions (relations (11), (13)–(17)) and amplitude (the ratio (12), (13)–(16), (18)) anisotropy of polycrystalline bile films. Figures 4 and 5 show results of the Jones-matrix reconstruction of phase distributions (relations (11), (13)–(17)) and amplitude (the ratio (12), (13)–(16), (18)) anisotropy of synovial fluid from the knee joint.

3.3.1. *Polycrystalline structure of bile films*

The analysis of the obtained results revealed the next features

- The presence of all types of optical anisotropy (see Figs. 2 and 3, (2), (3), (7), (8), respectively) for polycrystalline bile films of both groups. The histograms of the distributions are characterized by significant ranges of variation of the "birefringence $\left({}^{\Delta LB\, =\, 0rad\, \div\, 0.06rad;}_{\Delta CB\, =\, 0rad\, \div\, 0.09rad} \right)$ — dichroism $\left({}^{\Delta LD\, =\, 0rad\, \div\, 0.04rad;}_{\Delta CD\, =\, 0rad\, \div\, 0.06rad} \right)$" (see Figs. 2 and 3, (4), (5), (9), (10), respectively).
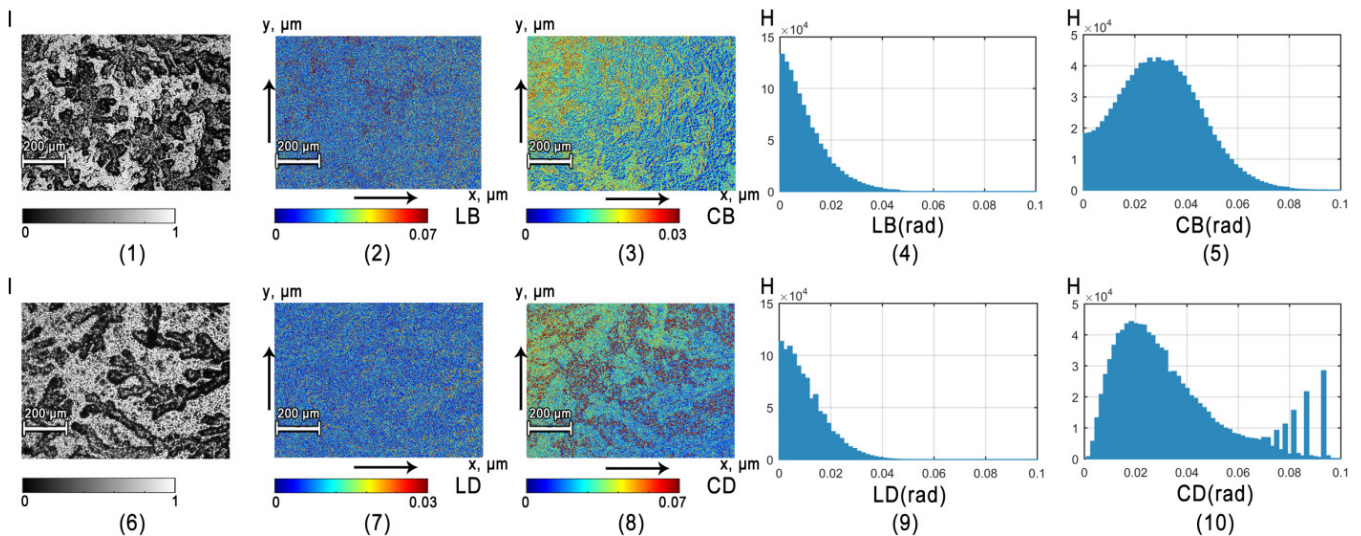

Fig. 2. Maps of intensity (1, 6), linear (2, 7) and circular (3, 8) birefringence; histograms of the phase anisotropy parameters (4, 5), (9, 10) of polycrystalline bile films of patients from group 1 (1)–(5) and group 2 (6)–(10).
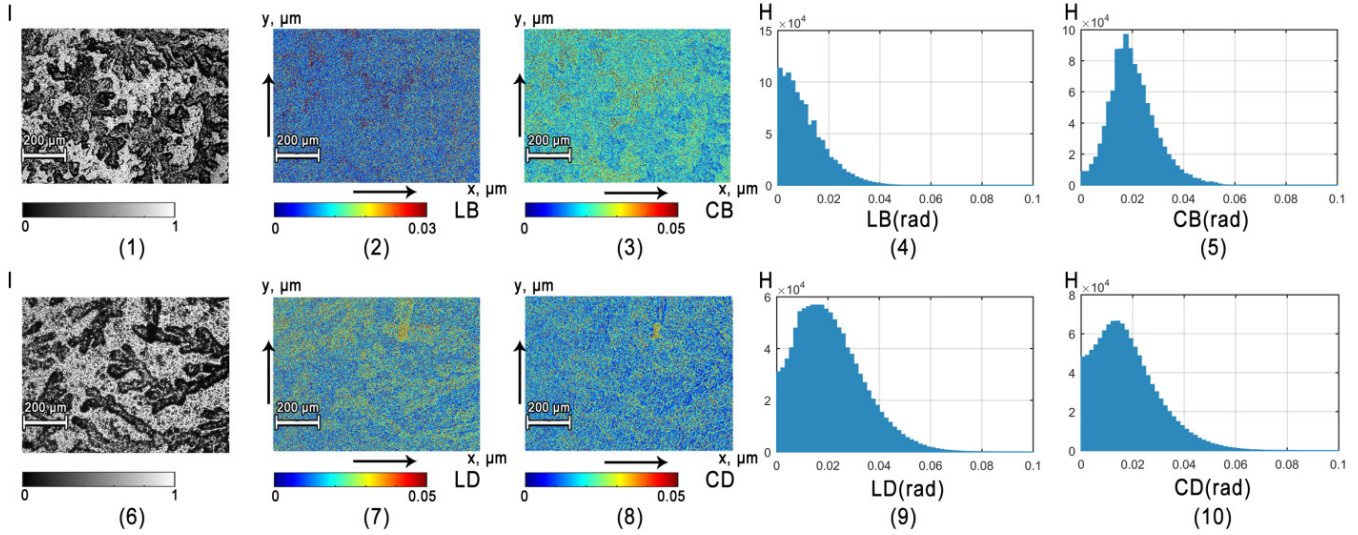
Fig. 3.   Maps of intensity (1, 6), linear (2, 7) and circular (3, 8) dichroism; histograms of the distribution of the parameters of the amplitude anisotropy (4, 5, 9, 10) of polycrystalline bile films of patients from group 1 (1)–(5) and group 2 (6)–(10).

- The predominance of optical activity and circular dichroism (see Figs. 2 and 3, (3),(8)) over the mechanisms of linear birefringence and dichroism (see Figs. 2 and 3 (2), (7)) of polycrystalline structures of bile films. The main extrema of the histograms H(CB) and H(CD) are localized in the region of large values CB and CD (see Figs. 2 and 3 (5), (10)) in comparison with the analogous distributions of H(LB) and H(LD) (see Figs. 2 and 3 (4), (9)). As a result, the distribution of circular anisotropy parameters is characterized by large values of the mean values $\bar{CB} \succ \bar{LB}$ (see

Fig. 2 (4), (5), (9), (10)) and $\bar{CD} > \bar{LD}$ (see Fig. 3 (4), (5), (9), (10)).

- The predominance of the optical activity (see Fig. 2 (3), (8)) of polycrystalline bile films from group 2 ("CLS") in comparison with the samples from group 1. The histograms H(CB) illustrate the growth (the presence of additional extremes $CB_{max} = 0.07\text{rad} \div 0.09\text{rad}$) of circular birefringence of bile samples in patients (see Fig. 2 (5), (10)). A similar but less pronounced picture is also observed for distributions of circular dichroism H(CD) (see Fig. 3 (5), (10)). As a result, for

Fig. 4.   Maps of intensity (1, 6), linear (2, 7) and circular (3, 8) birefringence; histograms of the distribution of the phase anisotropy parameters (4, 5, 9, 10) of polycrystalline synovial fluid films of patients from group 3 (1)–(5) and group 4 (6)–(10).
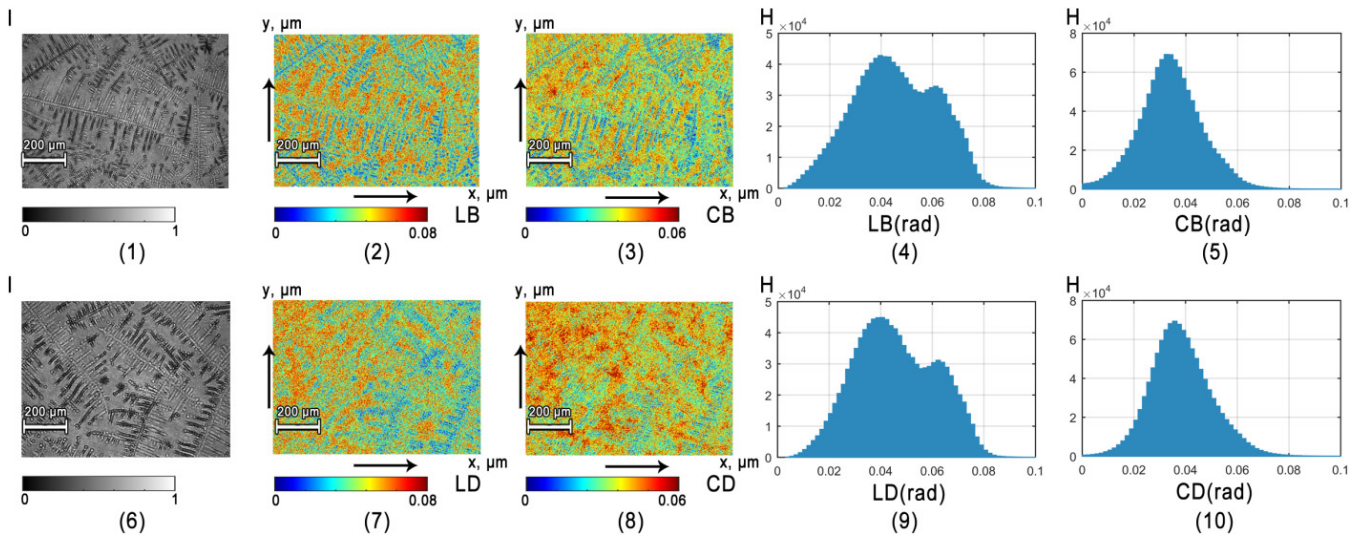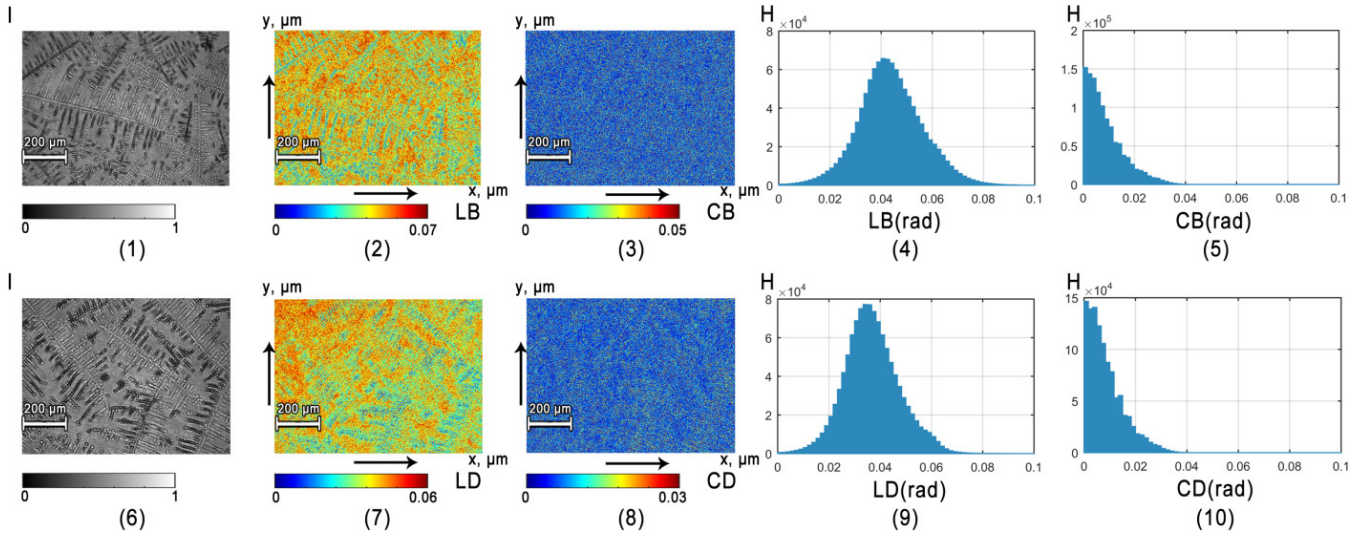
Fig. 5.   Maps of intensity (1, 6), linear (2, 7) and circular (3, 8) birefringence; histograms of the distribution of the phase anisotropy parameters (4, 5, 9, 10) of polycrystalline synovial fluid films of patients from group 3 (1)–(5) and group 4 (6)–(10).

the average values of the parameters of the circular phase and amplitude anisotropy of the bile films from both groups, the following relations can be written:

$$C\bar{B}(\text{"CLS"}) > C\bar{B}(\text{Norm});$$
$$C\bar{D}(\text{"CLS"}) > C\bar{D}(\text{Norm}) \tag{20}$$

These relations can be explained by the following reasons. The first, one, the polycrystalline component of the bile film contains a high concentration of optically active cholesterol monohydrate and calcium bilirubinate comparing to the linearly birefringent needle crystals of fatty acids. As a result, the mechanisms of circular phase anisotropy prevail over linear birefringence. Second, in the blue region of the spectrum, the absorption of molecular bile complexes is sufficiently larger.[42] Therefore, the predominance of circular dichroism is also quite pronounced. Third, the increase in circular birefringence and circular dichroism in the early stages of "CLS" can be associated with an increase in the concentration of cholesterol monohydrate and calcium bilirubinate.

3.3.2.   Polycrystalline structure of synovial fluid films

For the polycrystalline structure of synovial fluid films, as well as for the bile films (see Figs. 2 and 3 (4), (5), (9), (10)), all types of optical anisotropy are typical (see Figs. 4 and 5 (4), (5), (9), (10)). On the other hand, the mechanisms of phase anisotropy (see Fig. 4 (2), (3), (7), (8)) prevail over the optically anisotropic absorption (see Fig. 5 (2), (3), (7), (8)). This is indicated by the ranges of variation (ΔLB; ΔCB = 0rad ÷ 0.08rad and ΔLD = 0rad÷ 0.07rad; ΔCD = 0rad ÷ 0.04rad) as well as by localization of the main extremes (LB$_{\max}$ = 0.037rad; CB$_{\max}$ = 0.036rad and LD$_{\max}$ = 0.034rad; CD$_{\max}$ = 0rad) histograms H(Ph) (see Fig. 4 (4), (5), (9), (10)) and H(Am) (see Fig. 5 (4), (5), (9), (10)).

The pathological state of the knee joint leads to an increase of polycrystalline synovial fluid films linear birefringence from Group 2 (see Fig. 4 (4), (9)). Histograms H(LB) are characterized by large values of the main extremes (see Fig. 4 (9)) – LB$_{\max}^{(1)}$ = 0.042rad and LB$_{\max}^{(2)}$ = 0.063rad compared to similar distributions for samples from Group 1 (see Fig. 4 (4)).

Described features of the transformation of the polycrystalline structure of synovial fluid films can be explained by the following reasons. The first one is the fact that in the synovial fluid of the pathologically altered joint ("SA"), the concentration of fibrillar protein structures increases. As a result, the level of linear birefringence also increases.[43] Second, in the blue region of the spectrum, the absorption of the main protein complexes of the synovial fluid is rather small.[44] Therefore, the effects of optically anisotropic absorption are less pronounced in comparison with the mechanisms of phase anisotropy.

Table 1. Parameters of the statistical analysis of Jones-matrix tomograms of polycrystalline bile films.

Parameters	LB		CB	
	Group 1	Group 2	Group 1	Group 2
$Z_1 \times 10^{-3}$	$0.17 \pm 0.011^*$	$0.24 \pm 0.015^*$	$0.36 \pm 0.019^*$	$0.52 \pm 0.029^*$
$Z_2 \times 10^{-3}$	0.21 ± 0.012	0.32 ± 0.018	0.41 ± 0.023	0.59 ± 0.032
Z_3	$0.37 \pm 0.022^*$	$0.49 \pm 0.028^*$	$0.38 \pm 0.022^*$	$0.56 \pm 0.029^*$
Z_4	$0.51 \pm 0.027^*$	$0.76 \pm 0.044^*$	$0.31 \pm 0.017^*$	$0.49 \pm 0.026^*$
Parameters	LD		CD	
	Group 1	Group 2	Group 1	Group 2
$Z_1 \times 10^{-3}$	$0.09 \pm 0.006^*$	$0.12 \pm 0.008^*$	$0.14 \pm 0.009^*$	$0.21 \pm 0.013^*$
$Z_2 \times 10^{-3}$	0.11 ± 0.006	0.14 ± 0.008	0.16 ± 0.009	0.24 ± 0.0015
Z_3	0.43 ± 0.024	$0.35 \pm 0.0.19$	$0.37 \pm 0.021^*$	$0.21 \pm 0.012^*$
Z_4	0.66 ± 0.035	0.53 ± 0.028	$0.51 \pm 0.031^*$	$0.36 \pm 0.022^*$

3.4. *Statistical analysis*

Here, we present the results of statistical analysis of data from Jones-matrix tomography of polycrystalline structure $(\mathrm{OA} \equiv \left\{ {Ph(m \times n); \atop Am(m \times n)} \right\})$ of bile and synovial fluid films.

The differentiation between the control groups ("1"; "3") and investigated groups ("2"; "4") was determined by using the following methodology[45,46]:

- Within each set of values of statistical moments $Z_{i=1;2;3;4}$ (see Eq. (19)), we determined the average value $\tilde{Z}_{i=1;2;3;4}$ and standard deviation $\sigma_{i=1;2;3;4}$;
- Differences between the statistical sets $Z_{i=1;2;3;4}$ were significant in the case when the average value $\tilde{Z}_{i=1;2;3;4}$ within the control group did not "overlap" with the standard deviation $\sigma_{i=1;2;3;4}$ within investigated group and vice versa;
- Within both groups of biological tissues samples, the cutoff of 3σ (99.72% of all possible values of changes of Z_i) was chosen for the distribution of values of each statistical moments $\tilde{Z}_{i=1;2;3;4}$. Sequentially, we determined the number of "false negative" (b) and "false positive" (d) conclusions;
- For each statistical moment, the operational characteristics traditional for probative medicine[45–47] were calculated: sensitivity ($\mathrm{Se} = \frac{a}{a+b} 100\%$), specificity ($\mathrm{Sp} = \frac{c}{c+d} 100\%$) and balanced accuracy ($\mathrm{Ac} = \frac{\mathrm{Se} + \mathrm{Sp}}{2}$) were determined, where a is a number of "truly positive" conclusions within group ("1"; "3"); c is a number of "truly negative" conclusions within group ("2"; "4").

- The statistical moment for which the value of balanced accuracy Ac is maximal was used as a diagnostic criterion.

3.4.1. *Polycrystalline bile films*

The comparative analysis of obtained data showed that the differences between the values of average moments of all orders are statistically valid (Table 1).

The moments $Z_{i=1;3;4}$ (CB) and $Z_{i=1;3;4}$ (CD) appeared to be sensitive for differentiation of circular birefringence ($CB(m \times n)$) and dichroism maps ($CD(m \times n)$) of polycrystalline bile films (marked by * in Table 1). For linear birefringence and dichroism, the Jones-matrix tomograms $LB(m \times n); LD(m \times n)$ of bile films are less informative. The differences between both groups of bile samples are not so vivid.

Table 2 presents the parameters of Jones-matrix tomography balanced accuracy value of polycrystalline bile film optical anisotropy of practically healthy donors and patients with "CLS".

Table 2. Parameters of the statistical analysis of Jones-matrix tomograms of polycrystalline bile films.

Parameters	Z_i	LB	CB	LD	CD
$\mathrm{Ac}(Z_i)$	Z_1	86%*	90%*	85%*	88%*
	Z_2	74%	76%	72%	75%
	Z_3	88%*	94%*	82%	91%*
	Z_4	86%*	95%*	84%	92%*

Table 3.   Parameters of the statistical analysis of Jones-matrix tomograms of polycrystalline bile films.

	LB		CB	
Parameters	Group 3	Group 4	Group 3	Group 4
$Z_1 \times 10^{-3}$	$0.42 \pm 0.026^*$	$0.53 \pm 0.032^*$	0.32 ± 0.018	0.36 ± 0.021
$Z_2 \times 10^{-3}$	0.51 ± 0.032	0.56 ± 0.036	0.29 ± 0.016	0.33 ± 0.018
Z_3	$0.29 \pm 0.027^*$	$0.63 \pm 0.038^*$	$0.21 \pm 0.034^*$	0.16 ± 0.028
Z_4	$0.42 \pm 0.037^*$	$0.71 \pm 0.054^*$	$0.25 \pm 0.046^*$	0.21 ± 0.037
	LD		CD	
Parameters	Group 3	Group 4	Group 3	Group 4
$Z_1 \times 10^{-3}$	0.29 ± 0.018	0.34 ± 0.023	0.11 ± 0.008	0.13 ± 0.009
$Z_2 \times 10^{-3}$	0.32 ± 0.018	0.38 ± 0.021	0.16 ± 0.009	0.18 ± 0.011
Z_3	0.25 ± 0.047	0.34 ± 0.073	0.63 ± 0.023	$0.51 \pm 0.029^*$
Z_4	0.47 ± 0.032	0.31 ± 0.048	0.82 ± 0.018	0.62 ± 0.021

The obtained results enable to suggest Jones-matrix tomography allows for high accuracy measurements. According to the criteria of probative medicine,[45–47] the parameters $\mathrm{Ac}(Z_1(\mathrm{OA})) = 85\% \div 90\%$ and $\mathrm{Ac}(Z_{3;4}(\mathrm{LB})) = 86\% \div 88\%$ correspond to good quality (marked by * in Table 2). The maximal level of accuracy has been for asymmetry and kurtosis, which characterizes the distributions of circular birefringence and dichroism — $\mathrm{Ac}(Z_{3;4} (\mathrm{CB; CD})) > 90\%$ correspond to high quality.

3.4.2.   *Polycrystalline films of synovial fluid*

The results of the statistical and operational analysis of the Jones-matrix tomograms of the films of synovial fluid from the knee joint of patients from both groups are presented in Tables 3 and 4.

The analysis of the obtained data allows to suggest that the most sensitive parameters (Table 3) to the changes in the polycrystalline structure of the synovial fluid are Z_1, Z_3 and Z_4, which characterize the average, skewness and kurtosis of the linear birefringence (LB) distribution (marked by * in Table 3).

Good $(\mathrm{Ac}(Z_1(\mathrm{LB})) = 86\%)$ and excellent $(\mathrm{Ac}(Z_{3;4}(\mathrm{LB})) > 90\%)$ accuracy of differential diagnosis of pathology of the knee joint has been achieved (marked by * in Table 4).

Similar studies were conducted for other biological fluids (Table 5)

- urine — practically healthy donors (43 samples) and patients with albuminuria (43 samples);
- cytological smear — practically healthy donors (41 samples) and patients with cervical cancer (41 samples);
- blood plasma — practically healthy donors (42 samples) and patients with non-alcoholic fatty liver disease (42 samples).

The obtained results allow suggesting that the method of Jones-matrix tomography of polycrystalline films of biological fluids of human organs with various pathologies can be perspective and a

Table 4.   Parameters of the statistical analysis of Jones-matrix tomograms of polycrystalline bile films.

Parameters	Z_i	LB	CB	LD	CD
$\mathrm{Ac}(Z_i)$	Z_1	$86\%^*$	68%	66%	64%
	Z_2	74%	70%	68%	65%
	Z_3	$92\%^*$	78%	78%	74%
	Z_4	$94\%^*$	80%	79%	72%

Table 5.   Parameters of the statistical analysis of Jones-matrix tomograms of polycrystalline bile films.

Fluid	Urine	Blood plasma	Cytological smear
Pathology	Albuminuria	Non-alcoholic fatty liver disease	Cervical cancer
Objective parameters	$Z_{2;3;4}$ (LD,CD)	$Z_{3;4}$ (LB)	$Z_{1;2}$ (CB)
Maximum balanced accuracy	94%	93%	91%

useful method for clinical applications. This is indicated by the high ($\geq 90\%$) level of balanced accuracy in the diagnosis of various diseases, not at the late,[32–37] but at the early stages of their occurrence. A further increase in the accuracy of diagnostics is possible by conducting systemic clinical studies of a significantly larger number of patients.

4. Conclusions

The investigation of efficiency of the developed technique of Jones-matrix-based polarization imaging polycrystalline films of biological fluids approach for diagnosis of the pathological conditions of human organs has been presented. The high-order statistical moments of distributions of linear and circular birefringence, dichroism and their variations are utilized for quantitative noninvasive assessment of the polycrystalline films of biological fluids. It was shown that distributions of phase and amplitude anisotropy formed by polycrystalline films of biological fluids of human organs with various pathologies can be used as the quantitative diagnostic parameters. Based on the obtained results, the differentiation criteria between the causes of reactive synovitis and septic arthritis, early stages of cholelithiasis, as well as other pathologies (cervical cancer, non-alcoholic fatty liver disease, renal albuminuria) were defined using the statistical (statistical moments of the 1st–4th order) analysis of Jones-matrix tomograms of polycrystalline structure of films of biological fluids. The suggested quantitative approach is fast enough (the time of getting the result is $t \leq 15$ min) compared to the other techniques currently used in clinical practice. In this way, the described method has a strong potential for application in histology for differentiation of pathology of various human organs. Thus, in order to implement this method into routine laboratory practice, numerous clinical tests are required in gastroenterology, traumatology, gynecology and oncology.

Acknowledgments

References

1. V. V. Tuchin, L. Wang, D. A. Zimnyakov, *Optical Polarization in Biomedical Applications*, Springer & Science Business Media, Luxembourg, 2006.

2. O. V. Angelsky, P. P. Maksimyak, V. Ryukhtin, S. G. Hanson, "New feasibilities for characterizing rough surfaces by optical-correlation techniques," *App. Opt.* **40**(31), 5693–5707 (2001).

3. O. V. Angelsky, A. P. Maksimyak, P. P. Maksimyak, S. G. Hanson, "Interference diagnostics of white-light vortices," *Opt. Expr.* **13**(20), 8179–8183 (2005).

4. S. L. Jacques, R. J. Roman, K. Lee, "Imaging superficial tissues with polarized light," *Las. Surg. Med.* **26**, 119–129 (2000).

5. A. Ushenko, A. Sdobnov, A. Dubolazov, M. Grytsiuk, Y. Ushenko, A. Bykov, I. Meglinski, "Stokes-correlometry analysis of biological tissues with polycrystalline structure," *IEEE J. Select. Top. Quant. Electron.* **25**(1), 1–12, (2019).

6. V. Shankaran, J. T. Walsh, Jr., D. J. Maitland, "Comparative study of polarized light propagation in biologic tissues," *J. Biomed. Opt.* **7**(3), 300–306 (2002).

7. W. S. Bickel, W. M. Bailey, "Stokes, Mueller matrices, and polarized light scattering," *Am. J. Phys.* **53**, 468–478 (1985).

8. G. Mueller *et al.*, (eds.), *Medical Optical Tomography: Functional Imaging and Monitoring*, Vol. IS11, SPIE Press, Bellingham, Washington (1993).

9. N. Ghosh, I. A. Vitkin, "Tissue polarimetry: concepts, challenges, applications, and outlook," *J. Biomed. Opt.* **16**, 110801 (2011).

10. S. L. Jacques, *Handbook of Biomedical Optics*, D. Boas, C. Pitris, and N. Ramanujam, Eds., CRC Press, Boca Raton, London, New York (2011), pp. 649–669.

11. N. Ghosh, M. F. G. Wood, I. A. Vitkin, *Handbook of Photonics for Biomedical Science*, V. V. Tuchin, (Ed.), CRC Press, Taylor & Francis Group, London (2010), pp. 253–282.

12. D. Layden, N. Ghosh, A. Vitkin, *Advanced Biophotonics: Tissue Optical Sectioning*, R. K. Wang and V. V. Tuchin, (eds.), CRC Press, Taylor & Francis Group, Boca Raton, London, New York (2013), pp. 73–108.

13. A. Vitkin, N. Ghosh, A. de Martino, *Photonics: Scientific Foundations, Technology and Applications*, D. L. Andrews, (ed.), Vol. IV, John Wiley & Sons, Inc., Hoboken, New Jersey (2015), pp. 239–321.

14. A. G. Ushenko, D. N. Burkovets, Y. A. Ushenko, "Polarization-phase mapping and reconstruction of biological tissue architectonics during diagnosis of pathological lesions," *Opt. Spectrosc.* **93**(3), 449–456 (2002).

15. O. V. Angelsky, A. G. Ushenko, Y. G. Ushenko, "Investigation of the correlation structure of biological tissue polarization images during the diagnostics of their oncological changes," *Phys. Med. Biol.* **50**(20), 4811 (2005).

16. O. V. Angel'skiĭ, A. G. Ushenko, A. D. Arkhelyuk, S. B. Ermolenko, D. N. Burkovets, "Scattering of laser radiation by multifractal biological structures," *Opt. Spectrosc.* **88**(3), 444–447 (2000).

17. A. G. Ushenko, "Laser diagnostics of biofractals," *Quant. Electron.* **29**(12), 1078 (1999).

18. V. Ushenko, A Sdobnov, A. Syvokorovskaya, A. Dubolazov, O. Vanchulyak, A. Ushenko, I. Meglinski, "3D Mueller-matrix diffusive tomography of polycrystalline blood films for cancer diagnosis," *Photonics*, **5**(4), 54 (2018)

19. S. Y. Lu, R. A. Chipman, "Interpretation of Mueller matrices based on polar decomposition," *J. Opt. Soc. Am. A* **13**(5), 1106–1113 (1996).

20. S. ManhasM. K. Swami, P. Buddhiwant, N. Ghost, P. K. Gupta, K. Sighn, "Mueller matrix approach for determination of optical rotation in chiral turbid media in backscattering geometry," *Opt. Express*, **14**(1), 190–202 (2006).

21. M. K. Swami, S. Manhas, P. Buddhiwant, N. Ghost, A. Uppal, P. K. Gupta, "Polar decomposition of 3× 3 Mueller matrix: a tool for quantitative tissue polarimetry," *Opt. Express*, **14**(20), 9324–9337 (2006).

22. S. Manhas, M. K. Swami, H. S. Patel, A. Uppal, N. Ghosh, P. K. Gupta, "Polarized diffuse reflectance measurements on cancerous and noncancerous tissues," *J. Biophotonics*, **2**(10), 581–587 (2009).

23. Yu. A. Ushenko, V. A. Ushenko, A. V. Dubolazov, V. O. Balanetskaya, N. I. Zabolotna, "Mueller-matrix diagnostics of optical properties of polycrystalline networks of human blood plasma," *Opt. Spectrosc.* **112**(6), 884–892 (2012).

24. Yu. A. Ushenko, A. V. Dubolazov, V. O. Balanetskaya, A. O. Karachevtsev, V. A. Ushenko, "Wavelet-analysis of polarization maps of human blood plasma," *Opt. Spectrosc.* **113**(3), 332–343 (2012).

25. V. O. Ushenko, "Spatial-frequency polarization phasometry of biological polycrystalline networks," *Optic. Memory and Neural Networks*, **22**(1), 56–64 (2013).

26. V. A. Ushenko, N. D. Pavlyukovich, L. Trifonyuk, "Spatial-frequency azimuthally stable cartography of biological polycrystalline networks," *Intern. J. Opt.* **2013**, 7 (2013).

27. A. V. Dubolazov, N. V. Pashkovskaya, Yu. A. Ushenko, Yu. F. Marchuk, V. A. Ushenko, O. Yu. Novakovskaya, "Birefringence images of polycrystalline films of human urine in early diagnostics of kidney pathology," *Appl. Opt.* **55**, B85–B90 (2016).

28. A. G. Ushenko, N. V. Pashkovskaya, O. V. Dubolazov, Y. A. Ushenko, Y. F. Marchuk, V. A. Ushenko, "Mueller matrix images of polycrystalline films of human biological fluids," *Roman. Rep. Phys.* **67**(4), 1467–1479 (2015).

29. V. A. Ushenko, A. V. Dubolazov, L. Y. Pidkamin, M. Yu. Sakchnovsky, A. B. Bodnar, Y. A. Ushenko, A. G. Ushenko, A. Bykov, I. Meglinski, "Mapping of polycrystalline films of biological fluids utilizing the Jones-matrix formalism," *Laser Phys.* **28**, 025602 (2018).

30. R. A. Chipman, *Handbook of Optics*, Vol. 2: *Devices, Measurements, and Properties*, 2nd edition, McGraw-Hill Professional, 2nd ed., United States, (1994).

31. O. Artega, A. Canillas, "Analytic inversion of the Mueller-Jones polarization matrices for homogeneous media," *Opt. Lett.* **35**, 559–561 (2010).

32. European Diabetes Policy Group, "A desktop guide to Type 1 (insulin-dependent) diabetes mellitus," *Diabet Med.* **16**, 716–730 (2005).

33. S. S. Hamdulay, S. J. Glynne, A. Keat, "When is arthritis reactive?," *Postgrad. Med. J.* **82**(969), 446–453 (2006).

34. V. Abeysuriya, K. I. Deen, N. M. Navarathne, *Hepatobiliary Pancreat. Dis. Int.* **9**(9), 248–253 (2010).

35. J. Rovensky, E. Simorova, Z. Radikova, R. Imrich, "Biliary microlithiasis, sludge, crystals, microcrystallization, and usefulness of assessment of nucleation time," *Endocr. Regul.* **40**(2), 29–36 (2006).

36. P. J. Coutlakis, W. N. Roberts, and C. M. Wise, "Another look at synovial fluid leukocytosis and infection," *J. Clin. Rheumatol.* **8**(2), 67–71 (2002).

37. N. Presle, P. Pottie, H. Dumond, "Differential distribution of adipokines between serum and synovial fluid in patients with osteoarthritis. Contribution of joint tissues to their articular production," *Osteoarthr. Cartilage.* **14**(7), 690–695 (2006).

38. O. V. Angelsky, A. G. Ushenko, Yu. A. Ushenko, V. P. Pishak, A. P. Peresunko, *Handbook of Photonics for Biomedical Science*, CRC press, United States (2010), pp. 283–322.

39. Y. A. Ushenko, T. M. Boychuk, V. T. Bachynsky, and O. P. Mincer, *Handbook of Coherent-Domain Optical Methods*, Springer, Germany (2013), pp. 107–148.

40. M. R. Fish, *World Scientific Series in Contemporary Chemical Physics*, World Scientific, Singapore (2004), pp. 23.

41. R. Serivo, A. Sparado, V. Ressieri, and M. Bombardieri, "Soluble P-selectin levels in synovial fluid and serum from patients with psoriatic arthritis," *Reumatismo*, **57**(4), 250–255 (2005).

42. K. K. Giraev, N. A. Ashurbekov, M. A. Magomedov, A. A. Murtazaeva, and R. Medzhidov, "The effect of pathological processes on absorption and scattering spectra of samples of bile and pancreatic juice," *Opt. Spectrosc.* **119**(1), 162–170 (2015).

43. V. V. Tuchin, *Tissue Optics: Light Scattering Methods and Instruments for Medical Diagnostics*, 3rd Edition, Vol. PM 254, SPIE Press, Bellingham, Washington (2015).

44. D. S. Kliger, J. W. Lewis, E. C. Randall, *Polarized Light in Optics and Spectroscopy*, Academic Press, Boston (1990).

45. L. Cassidy, "Basic concepts of statistical analysis for surgical research," *J. Surg. Res.* **128**, 199–206 (2005).

46. C. S. Davis, *Statistical Methods of the Analysis of Repeated Measurements*, New York: Springer-Verlag (2002), pp. 744.

47. A. Petrie, B. Sabin, *Medical Statistics at a Glance*, Blackwell Publishing, United States (2005), pp. 157.